Electrical, Thermal, Structural and Optical Properties of $Li_{(x)}FeO_{2\,(1-x)}$ Nanorods and its Applications

V. Selvamurugan*, A. Arulsankar, P. Hemalatha, and M. Alagar
Centre for Research and P.G. Studies in Physics,
Ayya Nadar Janaki Ammal College (Autonomous), Sivakasi, India.

Abstract

Li doped iron oxide nanorods were synthesized by chemical co-precipitation method. XRD results are in good agreement with the JCPDS data. The crystallite size was calculated using Scherrer's formula. SEM studies brought out the surface morphology of prepared nanorods. The lithium doping to the iron oxide crystal lattice was confirmed through FTIR spectrum. Thermal properties of prepared nanorods were studied using DSC. The band gap of iron oxide nanorods was calculated from UV-absorption spectrum and is ascribed to quantum confinement effect. Electrical conductivity of the nanorods was determined using four probe method. The fluorescence spectrum was also recorded to elucidate the optical property of the prepared Iron nanorods.

Keywords - *XRD, SEM, FT-IR, DSC.*

1. Introduction

Nanotechnology is considered as a key to the 21st century. Nanotechnology promises have been assessed by various scientific communities. By meeting at the nanoscale, various disciplines, from physics via chemistry to biology, from engineering to medicine contribute synergistically to the newly created knowledge base and the resulting technological advances. The world is facing major challenges that cannot be sufficiently addressed by current technologies. These challenges include environmental protection, exploding health care expenses, as well as energy and resource limitations. Fabrication of metal and metal oxide nanostructure is found to be an emerging area in the field of nanoscience and nanotechnology [1].

Over the past few years, attention has been focused on the research field of one-dimensional nanostructural materials, such as nanorods or nanowires, because of their unique properties. These properties are derived from their low dimensionality, and their potential use in the interconnects and functional blocks that are used for fabricating nanoscale devices [2–4]. In general there are different ways to fabricate nanorods. Herein we report the synthesis of Li doped iron oxide nanorods using sodium hydroxide by chemical co-precipitation method and discussed the structural, optical, thermal properties and its applications.

2. Experimental Method

AR grade Ferric chloride anhydrous (m.wt.=162.21) and Lithium chloride anhydrous (m.wt.=42.39) from HiMedia were used as received.

$$FeCl_3 + LiCl + 2NaOH \xrightarrow{80°C} LiFeO_2 + 2NaCl + 2HCl$$

Ferric chloride and lithium chloride in mole percents were dissolved in de-ionized water. The concentration of Li ions was varied from 0 to 10%. The obtained solution was continuously stirred for 3 hours, and then maintained at 80^0C. NaOH was added drop by drop into the mixture and the resultant solution was continuously stirred for another one hour. After one hour, a precipitate began to form. Finally a reddish brown solution was obtained. The precipitate was separated using Wattmaan filter paper and the obtained precipitate was heated in a crucible upto 280°C for more than three hours to remove the moisture and other impurities. Finally FeO_2 nanoparticles doped with different Li concentrations were obtained. For comparison, pure FeO_2 nanoparticles were also prepared using the above method.

The samples were characterized by X-ray diffraction (XRD), Scanning Electron Microscopy (SEM), UV-VIS absorption spectroscopy, Differential Scanning Calorimetry (DSC), X-Ray fluorescence spectroscopy, fluorescence microscopy, Four probe conductivity and FTIR.

3. Results and Discussion

3.1Surface Morphology of $Li_{(x)}FeO_{2\,(1-x)}$

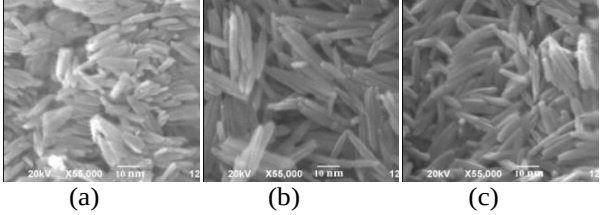

(a) (b) (c)

Figure 1. SEM Micrograph of the (a) 0 mol% (b) 5 mol% and (c) 10mol% lithium-doped FeO_2 nanorods.

Nanorods of uniform dimension were observed through SEM microscope (fig. 1). There is no agglomeration of nanorods are well ordered, uniform shape and dimension. From the SEM images, the size of $Li_{(x)}\ FeO_{2\ (1-x)}$ (for x= 0.0, 0.05, 0.10) nanorods was determined to be of the range ~ 10-12 nm. Further we inferred that the crystalline size has been decreased while increasing the lithium concentration.

3.2 Structural Analysis of $Li_{(X)}FeO_{2\ (1-X)}$ nanorods

X-ray diffraction (XRD) was performed with XPERT-PRO X-ray diffractometer at room temperature, using a quartz monochromator, Cu-kα radiation (λ=1.54060Å). Figure 2 shows the XRD pattern of $Li_{(X)}\ FeO_{2\ (1-X)}$ (where x= 0.0, 0.05, 0.10) nanorods. It was compared with the JCPDS file no. 89-7118 and is in good agreement with that of pure cubic-phase.

The XRD pattern of $Li_{(X)}\ FeO_{2\ (1-X)}$ nanorods showed the fundamental peaks due to the planes (111), (200), (220), (311). From the XRD analysis, no peaks of impurity phases were observed. Also, peak shift has been observed when comparing 5, 10 mol% samples and 0 mol% samples which confirm the presence of lithium atom in the FeO_2 crystal lattice. Due to size effect, XRD peaks were broadened and their width became larger as the particle had become smaller. The crystallite size (D) of $Li_{(X)}\ FeO_{2\ (1-X)}$ nanorods was calculated from the full-width at half maximum (FWHM) of XRD lines, using the Debye-Scherrer's formula.

$$D_{h,k,l} = 0.9\lambda/(\beta_{h,k,l}\cos\theta) \quad \ldots(1)$$

where D is the average crystalline diameter, λ is the wavelength in Angstrom, β is the Full width at half- maximum and θ is the Bragg angle. We used the most intense peak (200) in the XRD patterns to calculate the average crystalline size.

From table 1, it is clear that the particle size has been decreasing because of the smallest ionic radius of Li^{2+} (60pm) ions (being smaller than that of Fe^{2+} (76pm) ions) (radii size plays the main role) [5]. It is interesting that Fe^{2+} ions are replaced by Li^{2+} ions at the surface of the particles [6]. From this we conclude that Li^{2+} has been influencing the formation of Li doped iron oxide nanorods.

Table 1 Particle size from XRD

Doping level of Lithium	2θ in degrees	β x10^{-3} Radians	d-spacing (nm)	Average crystallite size from XRD (nm)	Average crystalline size from SEM (nm)
0	41.938	13.796	0.2155	10.76	11.95
0.05	43.633	15.368	0.2072	9.72	11.32
0.10	43.633	16.50	0.2072	9.05	10.13

From the XRD pattern, peak index were calculated by two different methods [7].

Table 2 Peak index calculated from Simple peak indexing method

Peak position 2θ (degree)	1000 Sin^{2}θ	1000 sin^{2}θ/35	Reflection	Remarks
37.533	103	3	(111)	$1^2+1^2+1^2=3$
43.633	138	4	(200)	$2^2+0^2+0^2=4$
63.383	276	8	(220)	$2^2+2^2+0^2=8$
77.03	388	11	(311)	$3^2+1^2+1^2=11$

Table 3 Peak index calculated from d-spacing

Peak position 2θ (degree)	d (Å)	1000/d^2	(1000/d^2)/ 59	(hkl)
37.533	2.394	174	3	(111)
43.633	2.072	233	4	(200)
63.383	0.1466	465	8	(211)
77.03	0.1237	654	11	(311)

Table 4 Experimental and standard diffraction angles of $Li_{(X)}\ FeO_{2\ (1-X)}$ nanorods

Experimental 2θ value (degree)	JCPDS 2θ value (degree)	Experimental (hkl) value	JCPDS (hkl) value
37.533	36.583	(111)	(111)
43.633	43.583	(200)	(200)
63.383	63.383	(211)	(211)
77.03	76.883	(311)	(311)

From table 4, it is obvious that the experimental and JCPDS values of θ and (hkl) values are perfectly matched. The XRD study confirmed that the resultant particles are $Li_{(X)}\ FeO_{2\ (1-X)}$ nanorods.

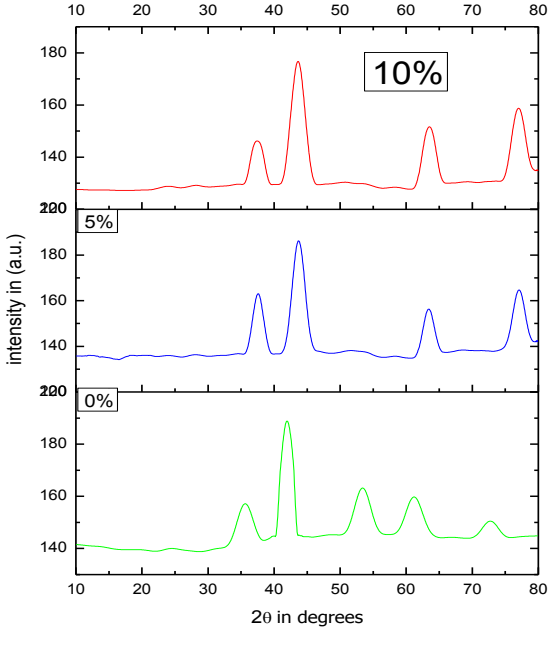

Figure 2. X-Ray diffractogram of prepared samples

3.3 DSC studies

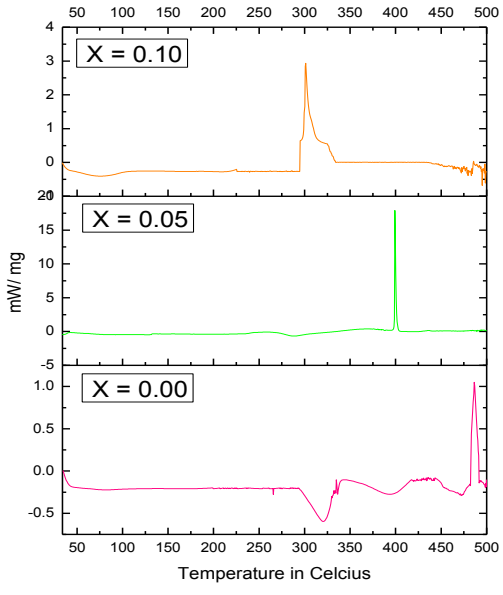

Figure 3. Differential Scanning Calorimetric Plot

Temperature versus power dissipated per weight of the sample is plotted using DSC Netzcho V-570 at the resolution of 0.5 degree, in the range of 35^{0}C to 500^{0}C. The figure 3 shows DSC graph for x= 0.0, 0.05, 0.10.

The prestine iron oxide in figure 3 showed one exothermic peak at 486.254^{0}C. Iron oxide doped with 5 mol. wt% and 10 mol. wt% of lithium showed an exothermic peak at 399.2^{0}C and 301.133^{0}C respectively.

Nanoparticles are employed for various applications, because of their remarkably lower melting temperature compared with bulk materials. These low melting temperatures of nanoparticles are due to the large ratio of surface atoms to inner atoms. This large ratio of surface atoms drastically decreases the melting temperature [8-9].

3.4 UV studies

The optical absorption spectra of undoped and doped iron oxide nanorods were characterized by UV-2400PC Series UV-Vis spectrophotometer in the range of 200 to 900nm with resolution of 2 nm are presented in figure 4.

From the UV-Visible studies, we conclude that the prepared nanoparticles have been used as UV absorption material because they absorb UV absorption rays. Since, the peak absorption is in the range from 850 to 900 nm, the prepared nanorods can be used in sun screen applications to stop far IR radiations.

In the figure 4, the strongest absorption peak of prepared sample for x =0.0 appears at 228 nm.

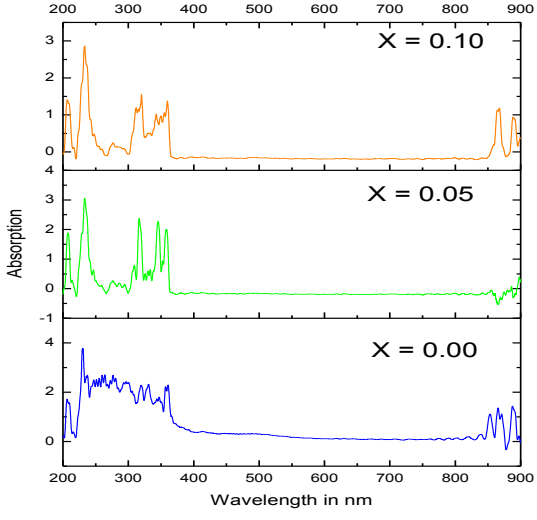

Figure 4. UV-Visible spectrum

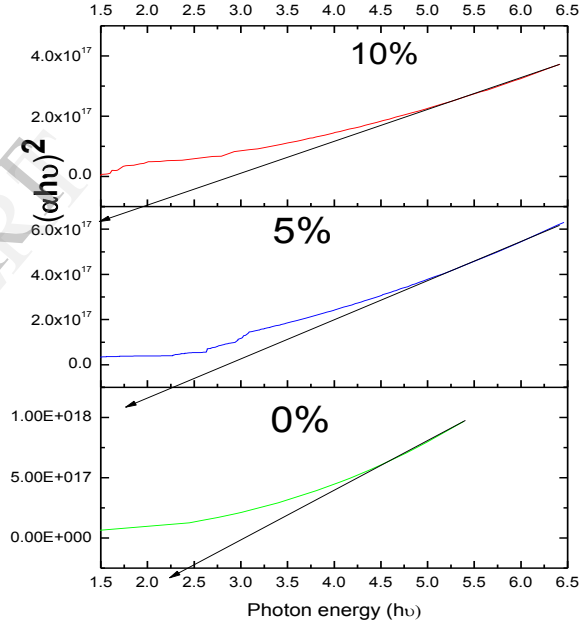

Figure 5. Tauc plot of prepared oxide nanorods (pure / doped) with Lithium nanorods

But for x = 0.05 and 0.10 the absorption peaks shifted towards red and appeared at 234 and 238 nm. The peak shifts are due to the quenching effect of the prepared nanorods.

The direct band gap energy was estimated from a plot of $(\alpha h\upsilon)^2$ versus photon energy ($h\upsilon$). The energy gap is determined using the relationship

$$\alpha h\upsilon = A(h\upsilon - E_g)^n$$

where, $h\upsilon$ = Photon energy, α = Absorption Coefficient, E_g = Energy band gap, n = ½ for the allowed direct band gap, n= 3/2 for direct forbidden band gap and n =2 for indirect band gap [10]. The direct band gap was obtained from extrapolating

the straight portion of the plot of $(\alpha h\upsilon)^2$ versus $(h\upsilon)$ as shown in figure 5.

Table 5. Band gap values for Li doped iron oxide nanorods

Doping level of lithium	Band gap energy in eV
0.0	2.45
0.05	2.25
0.10	2.00

The values of direct band gap (table 5) of the prepared nanorods are giving evidences for the sample as a semiconductor, since its energy band gap is in the range of 0 – 3 eV [11]. The decreasing value of band gap is due to the extra electron energy levels formed by the doping of lithium to iron oxide.

3.5 X-Ray Fluorescence Spectroscopic Studies

The fluorescence emission spectra of $Li_{(X)}$ $FeO_{2\ (1-X)}$ nanorods were examined by spectrofluorometer with resolution of 0.5 nm at an excitation wavelength of 228 nm and it is shown in figure 6. For x = 0.00, the fluorescence spectra gives only one emission peak at 352.5 nm.

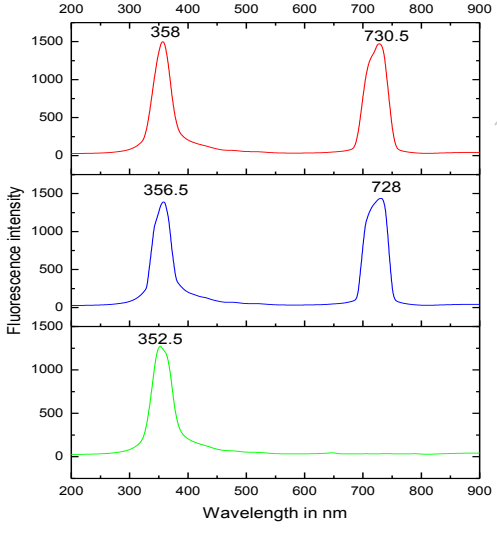

Figure 6. X-Ray fluorescence Spectrum

However, the emission spectrum for $Li_{(X)}$ $FeO_{2\ (1-X)}$ nanorods (for x =0.05 & 0.10) give two peaks. The additional peaks observed at 728 nm for x =0.05 and 730.5 nm for x =0.10 are due to the presence of Lithium. The small red-shift may be due to quenching effect [12]. Also, the fluorescent intensity changes with the concentration of Lithium. The fluorescence study confirmed that the Li doped iron oxide nanorods have enhanced fluorescence effect.

3.6 Fluorescence microscope studies:

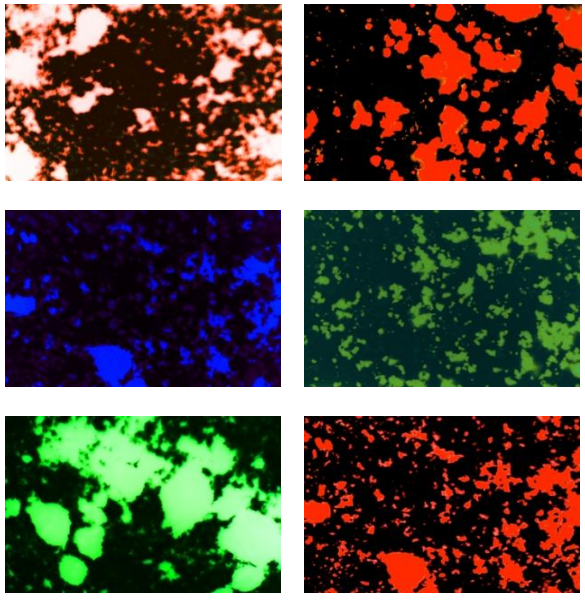

Figure 7. Fluorescence microscopic images of Lithium doped Iron oxide nanorods

Figure 7 shows the fluorescence optical microscope (Optika model B-353FL) bright field images of $Li_{(X)}$ $FeO_{2\ (1-X)}$ nanorods. From the fluorescence optical microscopic images, we can conclude the prepared nanorods can be used for fluorescence applications.

3.7 FT-IR studies

The figure 8 shows, the FTIR spectrum of the synthesized $Li_{(X)}$ $FeO_{2\ (1-X)}$ nanorods using 8400 SHIMADZU FTIR with resolution $2cm^{-1}$.

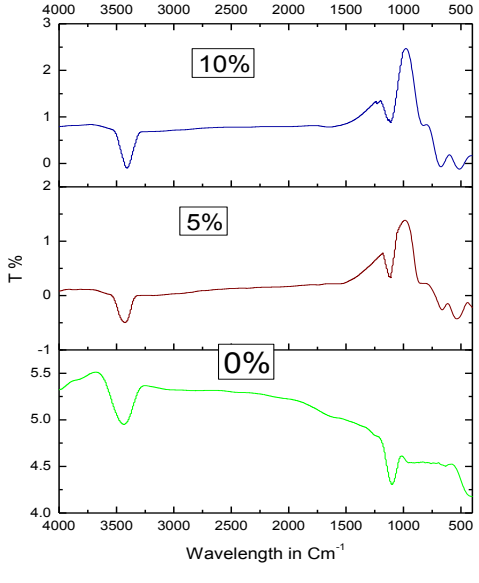

Figure 8. FTIR Spectrum

In the figure 8 (for x = 0.0) the absorption band at 1106 cm^{-1} [13, 14] is due to the FeO_2 nanorods, for x =0.05 and 0.10, the same peak is shifted to 1112 cm^{-1}. Also the appearance of new peaks around 536 and 652 cm^{-1} confirm the presence of lithium in the sample. Also, the increased doping level of lithium resulted in the increased intensity of absorption of the observed peaks.

Another peak at 3410cm^{-1} is assigned to the presence of adsorbed hydroxyl groups by the iron oxide nanorods [15].

3.8 Four Probe Conductivity Studies

The four probe conductivity measurement was taken using Scientific equipment, Roorkee, modal DFP-02 from room temperature upto 90°C.

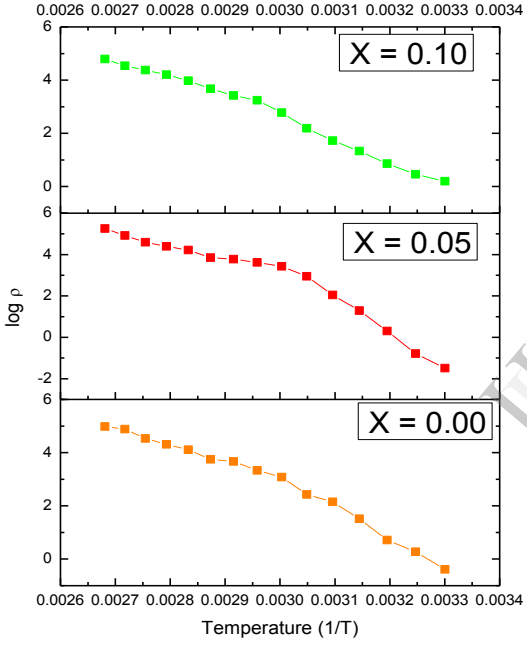

Figure 9. Arrhenius plot of iron oxide nanorods without and with lithium doping

The figure 9 shows the Arrhenius plot of $Li_{(X)}$ $FeO_{2\ (1-X)}$ nanorods. Thickness of the sample was 0.5 mm. The negative slope of the plot shows that the material is a semiconductor.

Table 6. Energy gap and Conductivity of prepared nanoparticles

Doping level	Resistivity Ohm cm	Conductivity S/cm	Energy gap from UV (ev)	Energy gap from Four probe conductivity (ev)
0%	244.3	4.09 x 10^{-3}	2.45	2.59
5%	283.3	3.47 x 10^{-3}	2.25	2.41
10%	1008	992.06 x 10^{-6}	2.00	2.26

A comparison between energy gap calculated by UV and Four Probe Conductivity measurements is shown in table 6. The calculated energy gap from Four Probe Conductivity studies agrees with that determined from UV studies.

4. Conclusion

Li doped Iron oxide nanorods were successfully synthesized by co-precipitation method and characterized by XRD, SEM, UV visible, FT-IR, Fluorescence, DSC and four probe conductivity method. From the structural characterization studies, we conclude that the prepared samples have simple cubic fcc structure. SEM images confirm the shape of the prepared samples to be nanorods. Spectroscopic studies revealed the presence of lithium and the outcome of UV and fluorescence studies imply their sunscreen and fluorescence applications. From thermal studies, the decrease in melting temperature indicated that the samples are in the nano regime. Four probe conductivity measurements complemented the energy band gap determined from UV studies.

References

1. H. Brune, H. Ernst, A. Grunwald, W. Grunwald, H. Hofmann, H. Krug, P. Janich, M. Mayor, W. rathgeber, G. Schmid, U. simon, V. Vogel, D. Wyrwa, and K. Madar., "Nanotechnology assessment and perspectives", Springer, (2006), pp 1-13.
2. J.T. Hu, M. Ouyang, P. Yang and C.M. Lieber, "Controlled Growth and Electrical Properties of Heterojunctions of Carbon Nanotubes and Silicon Nanowires" Nature, 399, (1999), pp 48.
3. D.S. Xu, G.L. Guo, L.L. Gui, Y.Q. Tang, Z.J. Shi, Z.X. Jin, Z.N. Gu, W.M. Liu, X.L. Li and G.H. Zhang, "Controlling growth and field emission property of aligned carbon nanotubeson porous silicon substrates", Applied Physics Letters, 75(4), (1999), pp 481-483.
4. J.R. Heath, P.J. Kuekes, G. Snyder and R.S. Williams, "A defect-tolerant computer architecture:Opportunities for nanotechnology", Science, 280, (1998), pp 1716- 1721.
5. H.Abdullah and S.A Halim, "Electrical and microstructure properties of $(La_{1-X}Pr_X)_{1/2}$ MnO_3 compounds", Sains. Malay, 23, (2009), pp213.
6. P.H.Borse, N.Deshmukh , R.F.Shinde , S.K.Date and S.K.Kulkarni, "Luminescence quenching in ZnS nanoparticles due to Fe and Ni doping", Journal of Material Science, 34, (1999), pp 6087-6093.
7. B.D.Cullity, "Elements of X-ray Diffraction", Addison-Wesley Pub.Co., (1978).
8. W. H. Qi and M. P. Wang, "Size effect on the cohesive energy of nanoparticle". Journal of Material Science Letter, 21,(2002), pp174.
9. K. K. Nanda, S. N. Sahu and S. N. Behera , "Liquid-drop model for the size-dependent melting of low-

dimensional systems", Physical Review A, **66**, (2002), pp. 013208.

10. P.K. Ghosh, Sk.F. Ahmed, S. Jana and K.K. Chottapadhyay, "Photoluminescence and field emission properties of ZnS:Mn nanoparticles synthesized by rf-magnetron sputting technique" Optical Materials, 29, (2007), pp.1584-1590.
11. W.H.Strehlow and E.L.Cook, Journal of Physical Chemistry, 2, (1973) ,pp 1-7.
12. H. Abdullah, S. Selmani, A. Roslan, S. Shaari, M. M. Salleh and JS. Mandeep, "Optical effect of Fe doped wurtzite ZnS nanoparticles", Advanced Research In Physics and Engineering, ISBN: 978-960-474-163-2, (2010), pp 191-194.
13. Aichun Dong and Winslow S.Caughey, "Infrared Methods for study of Hemoglobin reactions and structures", Methods in Enzymology, 32, (1994), pp 142.
14. Kazuo Nagamoto, "Infrared and raman spectra of inorganic and coordination compounds", fourth edition, John Wiley & Sons Limited, New York, (1986), pp. 316.
15. G. Kataby, A. Ulman, R. Prozorov, and A. Gedanken, "Coating of Amorphous Iron Nanoparticles by Long-Chain Alcohols, Langmuir, 14, (1998), pp 1512-1515.